sciendo

POLISH MARITIME RESEARCH 4 (116) 2022 Vol. 29; pp. 155-161
10.2478/pomr-2022-0053

A TRIBOELECTRIC NANOGENERATOR BASED ON A PENDULUM-PLATE WAVE ENERGY CONVERTER

Shenglin Zhu
Shaohui Yang*
Hui Li
Yan Huang
Zhichang Du
Jianyu Fan
Zhonghua Lin
College of Mechanical and Energy Engineering, Jimei University, Xiamen, China
Key Laboratory of Ocean Renewable Energy Equipment of Fujian Province, Xiamen, China
Key Laboratory of Energy Cleaning Utilization and Development of Fujian Province, Xiamen, China

* Corresponding author: *13163996278g@163.com (S. Yang)*

ABSTRACT

Ocean waves are a promising source of renewable energy, but harvesting this irregular low-frequency energy is challenging due to technological limitations. In this paper, a pendulum plate-based triboelectric nanogenerator (PP-TENG) is proposed. The PP-TENG absorbs wave energy through the pendulum plate installed at the bottom of the device, which generates a swing effect. This drives the motion of the upper TENG power generation unit and generates a charge transfer on the surface of a film of polymer PTFE and nylon, materials which are very sensitive to the low-frequency wave environment. The PP-TENG was tested after building a semi-physical simulation test platform. When the polymer materials were PTFE with a thickness of 0.01 mm and nylon with a thickness of 0.02 mm, 33 commercial LED lamps could be lit simultaneously. Moreover, under short-circuit conditions, the current reached 2.45 μA, and under open-circuit conditions, the voltage reached 212 V. When the PP-TENG was connected in series with a resistor with a resistance of 3 x 10^5 Ω, its maximum peak power density reached 6.74 mW/m^2. It can be concluded that the PP-TENG is characterised by low fabrication costs and excellent energy conversion efficiency. The combination of a pendulum wave energy converter with a TENG shows great output performance. This research lays a solid foundation for practical applications of the proposed structure in the future.

Keywords: TENG; wave energy; computer simulation; semi-physical simulation

INTRODUCTION

As the global energy supply becomes increasingly limited, reserves of traditional fuel, natural gas, coal, and other non-renewable energy sources are declining [1]. Issues related to energy supply can directly affect the future of human development, as production capacities and life itself are inseparable from the energy supply. Since traditional sources of energy will be exhausted sooner or later, and as these cause serious environmental pollution and climate change, it is necessary to find pollution-free sources of renewable energy [2]. The many forms of renewable energy include hydropower stations, wind energy (onshore/offshore), solar energy, material energy, geothermal, and tide and wave energy [3]. Of these, wave energy has the particular advantages of safety, lack of pollution, renewability, large reserves, and a wide distribution, and has therefore become a focus of attention in many countries [4]. Wave energy is a directly usable resource, with generation of approximately 32,000 TWh/year worldwide [5]. Scholars have recognised the immense energy contained in ocean waves, and have begun to work on developing and utilising this energy.

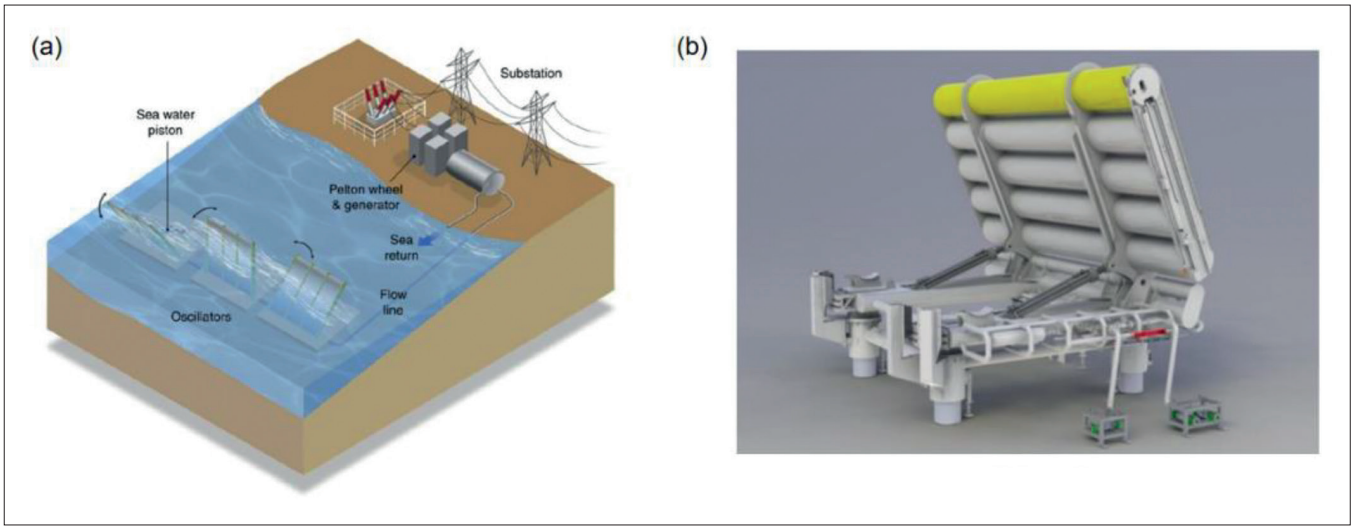

Fig. 1 Power generation systems using (a) a buoyancy pendulum [13] and (b) an EMG buoyancy pendulum [14]

In the early days, researchers focused on electromagnetic wave energy generators (EMGs). Lai conducted simulation experiments on the energy output of the oscillating float-type wave energy converter [6][7]. However, due to their bulky structure, EMGs have some natural drawbacks and are unsuitable for energy supply in small electronic equipment at sea [8]. A triboelectric nanogenerator (TENG) was proposed, and it was found that its power density was higher than that of EMGs (up to 3200 Wm-2) [9], the weight and production costs of the device were lower, and its low-frequency operation ability was better [10]. Moreover, a traditional EMG requires flotation devices (such as floats) due to its relatively large weight, while a TENG can easily float due to its smaller mass [11].

Wang invented the original version of the TENG, based on organic materials, in 2012 [12]. Its working principle was based on the coupling of triboelectric and electrostatic induction effects. A TENG was applied to the collection of wave energy for the first time in 2014 [10], and a significant amount of work has been done since then to improve the output efficiency of the TENG and to develop commercial applications for this technology. A variety of TENGs with improved power generation performance that can harvest ocean wave energy have also been designed, such as the spherical-shell structure [12], the wavy structure [13], the spring-assisted structure [14], the bionic structure [15], and the liquid-solid contact TENG [16]. Previous structural studies of EMGs found that pendulum structures have significant advantages in terms of absorbing wave energy [17]. In addition, Liang designed a spherical TENG structure based on wave energy [18], and realized the driving application of digital thermometer and water level detection. Zhang proposed a multi-gating structure of TENG, its power density can reach 4.2 mW/m^2 at a wave frequency of 0.5 Hz [19]. In the recent research progress of ocean wave energy collection TENG summarized by Huang, it can be seen that many structures have been verified to be feasible [20]. Some teams have tried to commercialise EMGs with this structure, and have achieved very good results [21]. Pendulum wave power generation exploits the interaction between a pendulum plate and a wave: the wave swings the pendulum plate around an axis, and its energy is converted into mechanical energy about the axis, which is used to drive a power generation device connected to the axis to generate electricity.

Existing studies have shown that the buoyant pendulum structure has extremely good efficiency for high-energy wave capture in shallow waters [22]. In areas with a wave period of 1.11 s and a wave energy density of 0.99 W/m, the efficiency of energy capture can reach 128% [23]. Based on the excellent wave energy conversion efficiency of pendulum wave energy collection device combined with TENG. The structure will play a huge role in offshore stationary wave energy harvesting devices, a structure called a PP-TENG is proposed in this paper, and a semi-physical simulation analysis is carried out.

STRUCTURE AND PRINCIPLE OF OPERATION OF PP-TENG

In this study, a simple TENG based on a pendulum-type structure is presented. The motion of the PP-TENG over a single wave cycle is shown in Fig. 2. The pendulum plate swings around the pendulum axis, and the TENG module is connected to the pendulum axis via hinges. The rotor acts as a motion unit, and is connected to the pendulum axis via hinges. The stator module is in a stationary state relative to the pendulum axis, while the rotor swings around the axis, thus forming a contact-sliding TENG structure between the rotor and the stator.

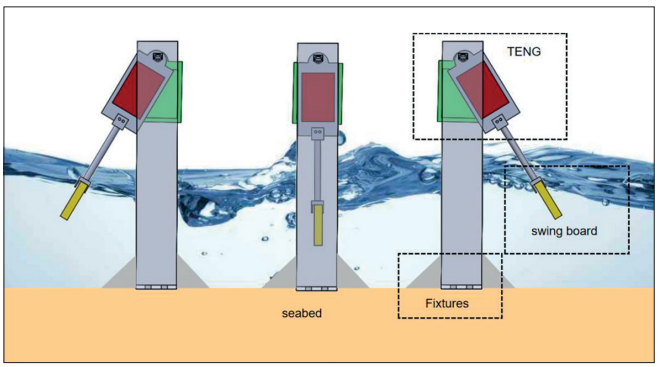

Fig. 2. Motion of the PP-TENG over a single wave cycle

The PP-TENG was designed to combine the advantages of a TENG with a pendulum wave energy power generation device. Its structure is shown in Fig. 3. A semi-physical simulation platform was built to simulate the influence of the swing and the initial charge density on the output performance of the PP-TENG and to evaluate its output performance.

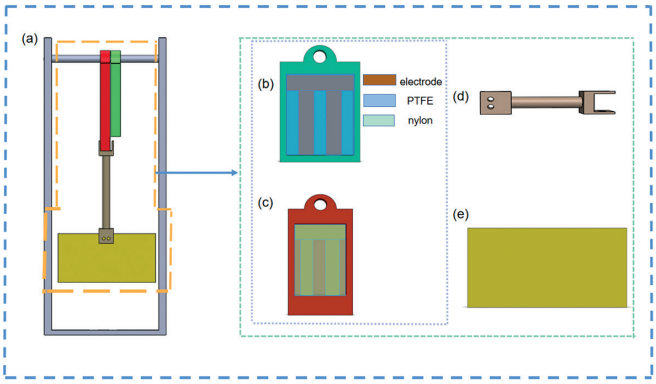

Fig. 3. (a) Schematic diagram showing the structure of the PP-TENG, (b) stator section, (c) rotor section, (d) connecting rod section, and (e) swinging board

The TENG theory has four modes: the vertical contact-separation mode, contact-sliding mode, single-electrode mode, and freestanding triboelectric-layer mode [24]. The PP-TENG is based on the contact-sliding mode. As shown in Fig. 4, two polymer materials overlap at the starting position and are in close contact with each other. Since polymer materials with different electronic capabilities are employed, triboelectric electrification causes them to have positive and negative charges on their surfaces. As shown in Fig. 4, when the positively charged upper plate starts to move, the contact area between the two plates decreases, separating the plane charges and hence increasing the potential of the upper plate. Driven by the potential difference, electrons will flow from the upper electrode to the lower to offset the potential difference generated by the triboelectric charge, thus forming a closed loop in a single motion cycle.

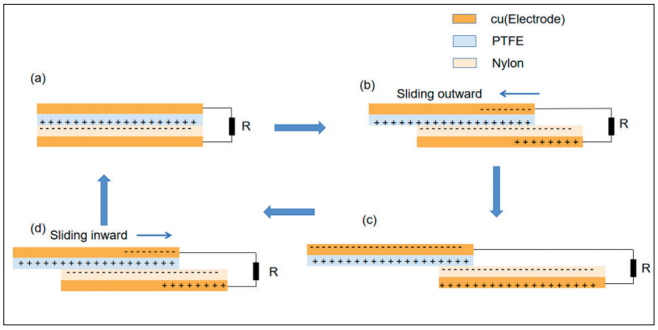

Fig. 4. Principle of operation of a TENG based on the contact-sliding mode: (a-d) TENG near short-circuit conditions after a complete motion cycle

SIMULATION OF THE ELECTRIC POTENTIAL FIELD

A simplified model of the PP-TENG was built using COMSOL Multiphysics to enable finite element calculations to be performed under open-circuit and short-circuit conditions. The effects of the swing variable θ on the open-circuit voltage output of the PP-TENG and the initial surface charge density on the transferred charge of the PP-TENG were visually demonstrated. This software is based on Maxwell's current displacement equation and the principle of electrostatic induction, and can be used to solve for the electric potential on the surface of the TENG polymer material throughout the motion cycle and the charge transfer on the surface.

Tab. 1. Basic parameters of the simulation model

Parameter	Length (mm)	Width (mm)	Thickness (mm)	Dielectric constant
Value	120	100	0.1	2.2

As shown in Table 1, the thicknesses of the electrode and polymer material are 0.1 mm, the length and width are 12 cm and 10 cm, and the polymer dielectric coefficient is set to 2.2. The initial charges are attached to the polymer surface to create an increase in the open circuit voltage of the PP-TENG, which differs for varying initial charges. The transferred charge at the electrode also changes to some extent under short-circuit conditions.

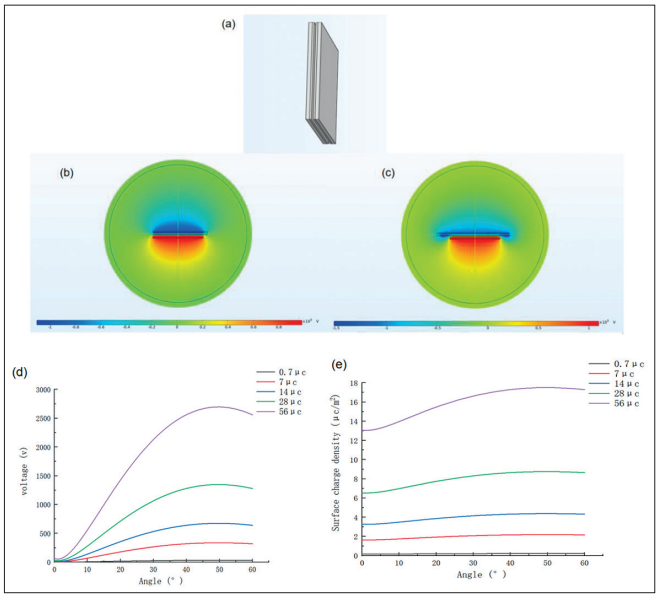

Fig. 5. (a) Simplified electric field model of the PP-TENG, (b) electrode surface potential distribution when the swing amplitude of the rotor is 45° (XY plane view), (c) electrode surface potential distribution when the swing angle of the rotor is 10° (XY plane view), (d) VOC-θ curve under open-circuit conditions with different initial surface charge densities, and (e) curves showing the surface charge density versus swing angle θ under short-circuit conditions with different initial surface charge densities

As shown in Fig. 5, the PP-TENG achieves a peak open-circuit voltage when the pendulum plate swing is approximately 45° while maintaining the surface charge density of the polymer material. The peak open-circuit voltage value gradually increases with the surface charge density. Figs. 5(b) and (c) show the potential distribution of the rotor in two different swing states. From Fig. 5(e), it can be seen that the surface transfer charge of the PP-TENG also peaks at a swing angle of the plate of around 45° under short-circuit conditions. This trend becomes more pronounced with an increase in the initial surface charge density. A semi-physical simulation test platform was built based

on the finite element simulation results for the electrostatic field to test the effects of external factors on the output performance of the PP-TENG.

EXPERIMENTAL METHODS AND INSTRUMENTS

DEVICE FABRICATION AND ASSEMBLY

The body of the PP-TENG consists of an external support frame, a pendulum plate, a connecting rod, and a pendulum shaft. The electrodes are attached to a substrate made of acrylic with a thickness of 4 mm and a length and width of 12 cm and 10 cm, respectively. The stator and rotor are made of 3D printed parts consisting of resin, and there are 10 x 12 cm slots on the stator and rotor that are used to fix the substrate. The pendulum plate is made of a 15 x 10 cm acrylic plate with a thickness of 10 mm. The plate is connected to the rotor via a connecting rod with a length of 10 cm and is installed on the guide rail of the linear motor through a living hinge. The power source is a 24 V linear reciprocating motor, and the external fixed frame is made of 30 x 70 cm aluminium profiles. As previously reported, the output voltage reaches its maximum value when the maximum displacement between two triboelectric materials is 10 times the thickness of the material [25]. Hence, PTFE with a thickness of 0.01 mm and nylon with a thickness of 0.02 mm were selected for the polymer materials. Finally, copper foil with a thickness of 0.05 mm was selected for the electrode. After the platform had been built, a Keithley 6514 electrometer was used as the measuring instrument.

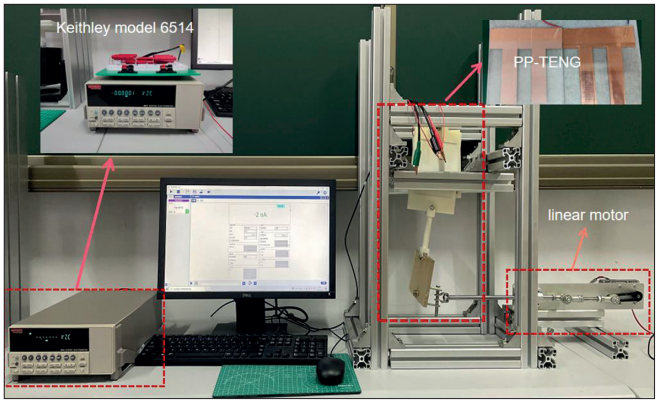

Fig. 6. Semi-physical simulation test platform for the PP-TENG

EXPERIMENTAL PROCEDURE

A 3D printer was used to create the stator and rotor models. An acrylic plate was employed as the base plate, with copper electrodes pasted on it, and the nylon and PTFE were attached to the surfaces of the electrodes. The substrate was placed in the pre-prepared groove on the model to form the power generation unit of PP-TENG. The pendulum plate and the rotor were connected via a connecting rod with a length of 13 cm to ensure consistency of movement. Lastly, the pendulum plate of the linear motor and the guide rod were connected via a living hinge.

The amplitude and frequency of swing of the plate were controlled by adjusting the feed speed and stroke of the linear motor, respectively. The feed speed of the motor was set to 60 rpm, and the swings of the plate was set to 15°, 30°, 45°, and 60°. The voltage under open-circuit conditions and the current under short-circuit conditions were measured for each group, and the surface of the polymer material of the DC high-voltage power supply for the PP-TENG was then pre-charged. Four control group experiments were carried out at zero, 5, 10, and 15 min. After obtaining the output performance of PP-TENG under open-circuit and short-circuit conditions, its output voltage, current, and power density were recorded under different loads to further verify its performance in practical applications. The PP-TENG was first used to light 33 commercial LED bulbs; it was then connected in series with loads characterised by different resistance values, and the output power was measured.

EXPERIMENTAL RESULTS AND DISCUSSION

The open-circuit voltage and the changes in the surface transfer charge with the swing amplitude under short-circuit conditions were obtained via a finite element simulation of the electrostatic field using COMSOL. A semi-physical simulation experimental platform was established, and experimental control groups were set up on this platform to further verify the simulation results. As shown in Fig. 7(a), the actual results from the operation of the PP-TENG show that the output voltage under open-circuit conditions has the highest value when the swing angle is 45°. At this point, the current peak value for the short-circuit condition reaches 2.45 μA, as shown in Fig. 7(b).

Our results show that the short-circuit current and open-circuit voltage output from the PP-TENG increase with the swing angle to reach a peak at 45°, and then undergo a gradual decrease. These experimental results agree with the output of the simulation, although the open-circuit voltage from the actual operation was slightly lower than the simulated result. The surface of the polymer material was pre-charged using a high-voltage DC power supply according to the conditions set in the previous simulation experiments (as shown in Fig. 7(c)). Thus, multiple experimental groups were set in the pre-charge period. As shown in Fig. 7(d), the amount of charge transferred from the surface is proportional to the amplitude of oscillation of the pendulum plate within a certain range. When the swing angle of the pendulum plate reaches 45°, the amount of charge transferred reaches a peak, and as the swing angle increases further, the charge transferred from the surface decreases. This trend becomes more pronounced when the initial charge on the polymer surface is increased. However, the growth rate slows after 10 min of charging due to the charge spillover effect, which is caused by the limited number of charge-carrying materials in the material.

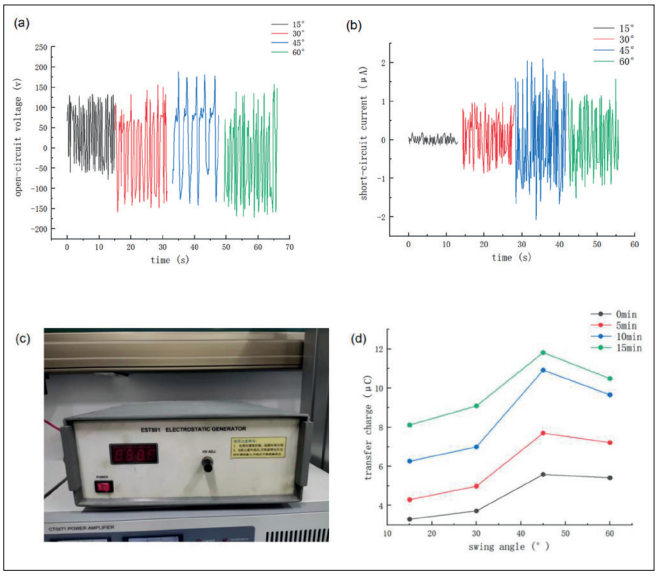

Fig. 7. (a) Magnitude of the output open-circuit voltage at different swing angles, (b) output short-circuit current for a swing angle of 45°, (c) the high-voltage DC power supply, and (d) surface transfer charges in the charged and uncharged states

Similar results were obtained from the computer simulations in which the PP-TENG was tested under open-circuit and short-circuit conditions, indicating that the PP-TENG structure has sufficient performance for practical applications. When the swing was 45°, the open-circuit voltage output from the PPTENG reached a peak value of 212 V, and the short-circuit current reached a peak value of 2.45 μA. When the polymer surface was charged with a high-voltage DC power supply, the surface transfer charge reached a maximum when the swing of PP-TENG was roughly 45°, as shown in Fig. 7(d). The surface transfer charge increased most rapidly at approximately 10 min, unlike in the simulation results. In view of the spillover effect of polymer charges during the experiment, the result obtained here is in line with expectations.

The PP-TENG was then connected in series to 33 LED bulbs to investigate its performance for practical applications, as shown in Fig. 8(a). It was observed that all 33 LEDs showed stable operation. Next, an external load circuit was built as illustrated in Fig. 8(b). Seven sets of test experiments with different external loads were set up. Based on the results, it could be concluded that the output voltage of the PP-TENG was positively correlated with the external load resistance within a certain range, while its output current was negatively related to the external load resistance, as shown in Fig. 8(c). The load that enabled the PP-TENG to generate the maximum output power under these experimental conditions was obtained by calculating the power of the PP-TENG, as shown in Fig. 8(d). It was found that under these preset experimental conditions, the load that could maximise the output power density of the PP-TENG was approximately 3 x 105 Ω. When the external load was less than this, the output power density of PP-TENG increased with the external load resistance, whereas when the external load exceeded 3 x 105 Ω, the output power density of PP-TENG increased as the load decreased. The load that maximised the output power density of the PP-TENG was obtained under these conditions, and can provide a reference environment for the practical application of the PP-TENG.

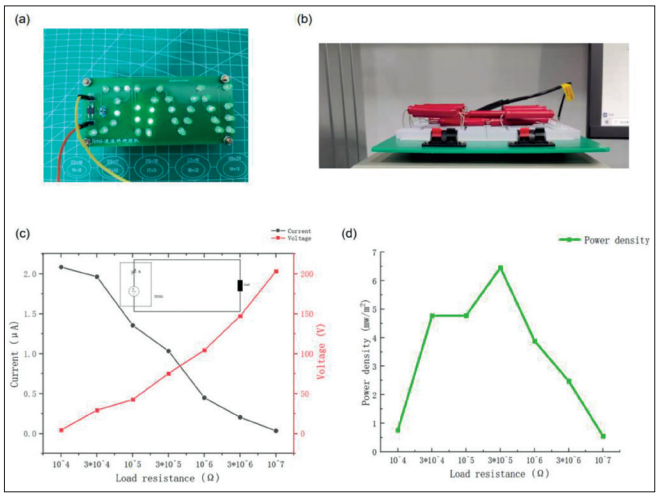

Fig. 8. (a) PP-TENG external load test circuit, (b) load resistance group, (c) the current flowing through different loads and the voltage changes at both ends, and (d) different power densities of PP-TENG under various loads

When the best matched load had been determined, multiple groups of controlled experiments were conducted at different swing frequencies under this load, and the results are shown in Fig. 9.

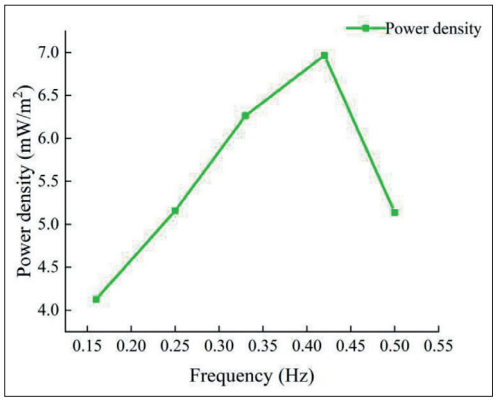

Fig. 9. Influence of swing frequency on the output power density of the PP-TENG for the best-matched load circuit

It was found that in the experimental environment of the physical simulation test bench, when the external resistance was best matched, the maximum peak power density could be obtained for an oscillation frequency of 0.42 Hz. Since this frequency is converted by the speed of the linear motor, there may be some deviation in the result. These conclusions were verified through a wave-making flume experiment.

CONCLUSIONS

In this study, we have presented a TENG based on a pendulum plate that absorbs wave forces in contact-sliding mode. This structure has low cost, high efficiency, and excellent electrical output performance. The rotor swing and the initial charge density effect of the open-circuit voltage VOC for open-circuit conditions were obtained based on the results of a finite element

calculation and COMSOL electrostatic field simulations. A semi-physical experimental simulation platform was established to simulate the swing angle and initial charge density and to allow us to experimentally evaluate the effect of external factors on the output performance of the PP-TENG. The results indicate that the PP-TENG almost reached the rated output at a swing angle of 45° with a power density of 6.74 mW/m^2. The PP-TENG also demonstrated adaptability to different surface charge densities, and was used to light up 33 LED bulbs simultaneously. The exchange charge density of the triboelectric materials used here, arising from the triboelectric charge exchange, was obtained as 4.73 μC. In this research, we considered only a semi-physical simulation experiment for the structure of the PP-TENG, which may show some differences from the actual performance in a wave environment. In future work, the output performance of the PP-TENG will be further studied using a wave-making flume, and will finally be put into operation in a sea test.

ACKNOWLEDGEMENTS

The authors would like to acknowledge support from the National Natural Science Foundation of China (Grant No. 51779104), the Natural Science Foundation of Fujian Province, China (Grant No. 2020J01694), and the Foreign Cooperation Program of Fujian Province, China (Grant No. 2020I0021).

REFERENCES

1. M. Liu, H. Liu, X. Zheng, H. Chen, L. Wang, and L. Zhang, "Nonlinear PTO effect on performance of vertical axisymmetric wave energy converter using semi-analytical method," *Polish Marit. Res.*, vol. 24, no. S3, 2017, doi: 10.1515/pomr-2017-0104.

2. Wave energy in the UK: Status review and future perspectives. Siya Jin, Deborah Greaves. doi.org/10.1016/j.rser.2021.110932

3. "Global oceanic wave energy resource dataset—with the Maritime Silk Road as a case study," doi.org/10.1016/j.renene.2021.01.058

4. W. Lai, Y. Xie, and D. Li, "Numerical study on the optimization of hydrodynamic performance of oscillating buoy wave energy converter," *Polish Marit. Res.*, vol. 28, no. 1, 2021, doi: 10.2478/pomr-2021-0005.

5. F. Taveira-Pinto, G. Iglesias, P. Rosa-Santos, and Z. D. Deng, "Preface to special topic: Marine renewable energy," *J. Renew. Sustain. Energy*, 7 (2015), 061601.doi.org/10.1063/1.4939086

6. Lai W, Xie Y, Li D. Numerical study on the optimization of hydrodynamic performance of oscillating buoy wave energy converter[J]. *Polish Maritime Research*, 2021.

7. Lai W, Li D, Xie Y. Simulation and experimental study of hydraulic cylinder in oscillating float-type wave energy converter[J]. *Polish Maritime Research*, 2020.

8. H. Shao et al., "Triboelectric-electromagnetic hybrid generator for harvesting blue energy," *Nano-micro Lett.*,vol. 10, no. 54, 2018.

9. F. R. Fan, W. Tang, Y. Yao, J. Luo, C. Zhang, and Z. L. Wang, "Complementary power output characteristics of electromagnetic generators and triboelectric generators," *Nanotechnology*, vol. 25, p. 135402, 2014.

10. G. Zhu et al., "A shape-adaptive thin-film-based approach for 50% high-efficiency energy generation through micro-grating sliding electrification," *Adv. Mater.*, vol. 26, pp. 3788–96, 2014, doi.org/10.1002/adma.201400021.

11. S. Niu et al., "Theory of sliding-mode triboelectric nanogenerators," *Adv. Mater.*, vol. 25, no. 43, pp. 6184-6193, 2013, doi.org/10.1002/adma.201302808.

12. X. Zhang et al., "Review of nano-phase effects in high strength and conductivity copper alloys," *Nanotechnology Reviews*, vol. 8, no. 1, pp. 383-395, 2019, doi.org/10.1515/ntrev-2019-0034.

13. T. Jiang et al., "Structural optimization of triboelectric nanogenerator for harvesting water wave energy," *ACS Nano*, vol. 9, no. 12, pp. 12562-12572, 2015, doi.org/10.1021/acsnano.5b06372.

14. L. Xu, et al., "Integrated triboelectric nanogenerator array based on air-driven mem-brane structures for water wave energy harvesting," *Nano Energy*, vol. 31, pp, 351-358, 2017, doi.org/10.1016/j.nanoen.2016.11.037.

15. J. Lucas, S. H. Salter, J. Cruz, R. J. M. Taylor, and I. Bryden, "Performance optimisation of a modified Duck through optimal mass distribution," in *Proceedings of the 8th European Wave and Tidal Energy Conference*, Uppsala, Sweden, 2009. pp. 7-9.

16. J. Liu, P. Fei, J. Zhou, R. Tummala, and Z. L. Wang, "Toward high output-power nanogenerator," *Appl. Phys. Lett*., vol. 92, p. 173105, 2008, doi.org/10.1063/1.2918840.

17. Y. Li and Y. H. Yu, "A synthesis of numerical methods for modeling wave energy converter-point absorbers," *Renewable and Sustainable Energy Reviews*, vol. 16, no. 6, pp. 4352-4364, 2012, doi.org/10.1016/j.rser.2011.11.008.

18. Liang X, Jiang T, Liu G, et al. Spherical triboelectric nanogenerator integrated with power management module for harvesting multidirectional water wave energy[J]. Energy & Environmental Science, 2020, 13(1): 277-285.

19. Zhang D, Shi J, Si Y, et al. Multi-grating triboelectric nanogenerator for harvesting low-frequency ocean wave energy[J]. Nano Energy, 2019, 61: 132-140.

20. Huang B, Wang P, Wang L, et al. Recent advances in ocean wave energy harvesting by triboelectric nanogenerator: An overview[J]. Nanotechnology Reviews, 2020, 9(1): 716-735.

21. L. Cameron, et al., "Design of the next generation of the Oyster wave energy converter," in *3rd International Conference on Ocean Energy*, ICOE Bilbao, Spain, 2010, vol. 6, p. 1e12.

22. K. Budal and J. Falnes, "Interacting point absorbers with controlled motion. power from sea waves," Edinburgh, UK, pp. 381-398.

23. M. Folley, MT. J. T. Whittaker, and A. Henry, "The effect of water depth on the performance of a small surging wave energy converter," *Ocean Engineering*, vol. 34, no. 8-9, pp. 1265-1274, 2007, doi.org/10.1016/j.oceaneng.2006.05.015.

24. Z. LináWang, "Triboelectric nanogenerators as new energy technology and self-powered sensors–Principles, problems and perspectives," *Faraday Discussions*, vol. 176, pp. 447-458, 2014, doi.org/10.1021/nn404614z.

25. H. Zou, Y. Zhang, L. Guo, P. Wang, X. He, G. Dai, H. Zheng, C. Chen, A. C. Wang, C. Xu, and Z. L. Wang, "Quantifying the triboelectric series," *Nat. Commun*., vol. 10, p. 1427, 2019.

CONTACT WITH THE AUTHORS

Shenglin Zhu

Shaohui Yang
e-mail: 13163996278g@163.com

Hui Li

Yan Huang

Zhichang Du

Jianyu Fan

Zhonghua Lin

College of Mechanical and Energy Engineering
Jimei University
Xiamen, 361021

Key Laboratory of Ocean Renewable
Energy Equipment of Fujian Province
Xiamen, 361021

Key Laboratory of Energy Cleaning Utilization
and Development of Fujian Province
Xiamen, 361021
China